NONLINEAR DROPLET DYNAMICS IN IDEALIZED TRAILING VORTICES

Orr Avni[1] & Yuval Dagan[1]

[1]Faculty of Aerospace Engineering, Technion – Israel Institue of Technology, Haifa, Israel

Abstract

This study investigates the dynamics of water droplets within a Batchelor vortex. Such an analytically described flow structure serves here as a model that may capture the essence of a trailing vortex. A Lagrangian approach is used to analyze the coupling between droplet motion and the flow field generated by the vortex. Under certain thermodynamic and hydrodynamic conditions, droplets may undergo evaporation and condensation when circulating the vortex core due to sharp changes in the environmental conditions induced by the vortex. The vortex-induced pressure drop is quantified using a non-dimensional vortex Euler number, revealing conditions required for condensation initiation within the vortex core. The onset of condensation is characterized by defining a mass transfer coefficient, indicating the direction and extent of mass transfer to the droplets. Our study uncovered a distinct clustering phenomenon linked to the initial Stokes number, with droplets showing a tendency to aggregate at higher Stokes numbers. The presented model may offer valuable insights into droplet dynamics within trailing vortices, contributing to improved modeling and prediction of droplet transport phenomena in the vicinity of trailing vortices.

Keywords: Trailing vortices, Droplet dynamics, Lagrangian analysis, Vortex-induced condensation.

1. Introduction

While the interactions between droplets and their environment are a fundamental problem in fluid mechanics [1, 2], our understanding of such phenomena is far from complete. The complexity of the general problem arises from the strong coupling between the carrier flow and the transport of mass, momentum, and heat to the droplet, thus limiting the scope of any general analysis. Past studies have thoroughly investigated the two-way coupling between simple vortices and droplets with a comparable length scale and found that these vortical structures could significantly alter the droplet evaporation rate in spray combustion systems [3–8]. Nevertheless, a large vortical structure might completely change the dynamics and thermal behavior of the single droplet [9–13].

A clear manifestation of such complex interactions is wingtip trailing vortices, which enhance the condensation and freezing of the air's vapor content and contribute to the formation of condensation trails. The resultant multiphase flow structures might alter the local radiative forcing and the photochemistry of the atmosphere [14]. The interaction between trailing vortices and dispersed particles may also influence the efficiency of aerial agricultural spraying, as the aircraft wake can alter the motion of the spray drops [15]. The analysis of multiphase trailing vortices using high-fidelity simulations may require the implementation of Lagrangian particle tracking. However, incorporating a detailed model might have high computational costs, even for relatively simple setups. Therefore, we offer a new Lagrangian analysis of the dynamics of droplets swirling within a simple, analytically described viscous vortical flow structure, the well-known Batchelor vortex. Batchelor [16] suggested an extension of such a similarity solution for modeling a trailing vortex far downstream from the wing itself owing to the complexity of such a three-dimensional unsteady problem [17].

Hence, our analysis aims to reveal the complex interaction between Batchelor's Lamb-Oseen-based vortex and a Lagrangian droplet as it may undergo both evaporation and condensation due to sharp changes in the environmental conditions generated by the vortex. The nonlinear relations between

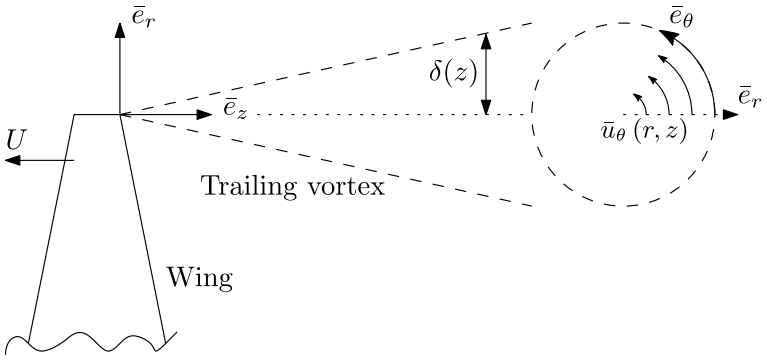

Figure 1 – Carrier flow setup.

the carrier flow fields, droplet relaxation time, drag forces, mass convection, and heat exchange will be derived and analyzed. The isolation of the interaction between the modeled vortical flow and the droplets allows for a rudimentary, parametric investigation of the transport processes. Thus, the proposed model offers a new analytic tool that might aid in uncovering the underlying physical mechanisms governing the fundamental problem of droplet evaporation and condensation within wingtip trailing vortical structures.

2. Governing Equations

The transport of discrete micron-sized droplets within a steady, analytically-described Batchelor vortex is analyzed here using a Lagrangian approach. The single droplet's spatial location $\boldsymbol{x}_p$, velocity $\boldsymbol{u}_p$, diameter d_p, and temperature T_p are traced and coupled to the local flow $\boldsymbol{u}_f$, pressure p_f, and temperature T_f fields. We assume the droplets are dispersed and dilute enough such that their motion does not affect the flow field; furthermore, any potential interactions between droplets are discounted. The equations for the carrier flow and the Lagrangian droplet are presented as follows.

2.1 Carrier flow

The investigated carrier flow, a three-dimensional Batchelor vortex, describes an axisymmetric vortical structure decaying due to viscous effects. The initial vortex intensity Γ is determined by the wing's geometry and the flight conditions. The customary time variable t is replaced here by U and z, the flight velocity and downstream distance from the wing, correspondingly. Assuming the trailing vortex system is generated by a wing on which the total drag force is D, the velocity field of such flow may be expressed in cylindrical coordinates as

$$\tilde{\mathbf{u}}_f = \left[\frac{\Gamma}{2\pi\tilde{r}}\left(1-e^{-\frac{U\tilde{r}^2}{4\nu_f\tilde{z}}}\right)\right]\bar{e}_\theta + \left[U - \frac{D}{8\pi\rho_f\nu_f z}e^{-\frac{U\tilde{r}^2}{4\nu_f\tilde{z}}}\right]\bar{e}_z\ . \tag{1}$$

when considering that the axial and azimuthal velocities decay independently [16]. Since the Batchelor vortex is an exact solution of the Navier-Stokes equation, we may extract an analytic expression for the pressure field induced by the vortical flow. As we investigate the droplets' dynamics near a vortical structure, this model assumes that the pressure drop is induced only by the circulation. The pressure term yields [17]

$$\tilde{p}_f = p_0 - \frac{\rho_f\Gamma^2}{8\pi^2\tilde{r}^2}\left[\left(1-e^{-\frac{U\tilde{r}^2}{4\nu_f\tilde{z}}}\right)^2 + \frac{U\tilde{r}^2}{2\nu_f\tilde{z}}\left(\mathrm{Ei}\left(\frac{U\tilde{r}^2}{4\nu_f\tilde{z}}\right) - \mathrm{Ei}\left(\frac{U\tilde{r}^2}{2\nu_f\tilde{z}}\right)\right)\right]\ , \tag{2}$$

given that p_0 is the far-field pressure and $\mathrm{Ei}(x) = \int_{-x}^{\infty} e^{-\xi}/\xi\ d\xi$ is the tabulated exponential integral notation.

We set c, the wing's chord length as the characteristic radial length, U as the characteristic velocity, and introduce the normalized variables

$$r = \tilde{r}/c; \quad z = \tilde{z}/c\mathrm{Re}_c; \quad \eta = r^2/4z; \quad u = \tilde{u}/U; \quad \tilde{p} = p/p_0, \tag{3}$$

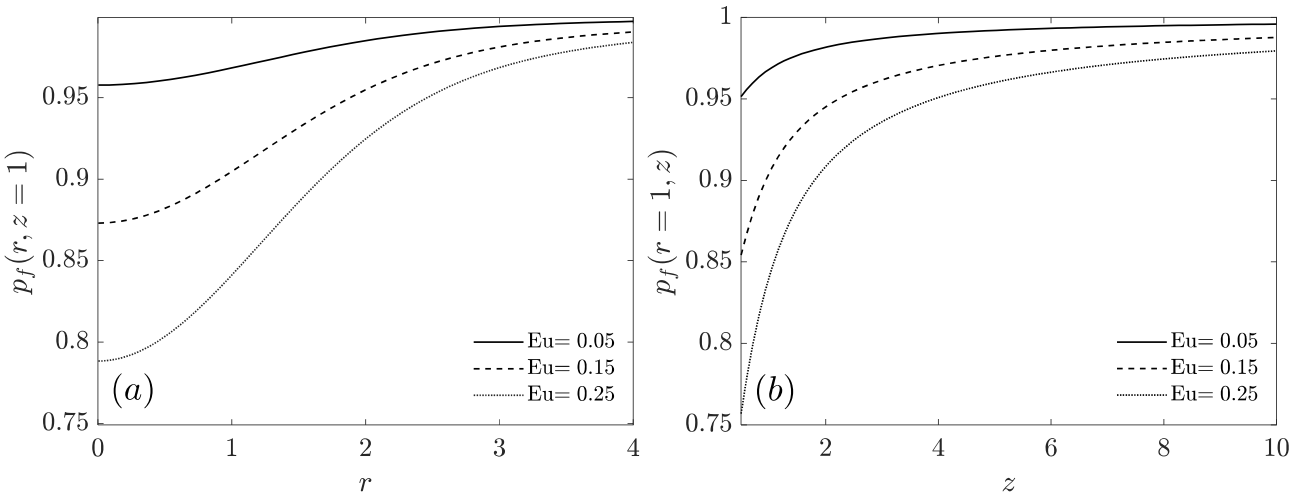

Figure 2 – Normalized pressure distribution $p_f(r,z)$ for various values of the non-dimensional Euler number Eu, as predicted by Eq. (5). (a) Radial pressure distribution at axial location $z = 1$. (b) Pressure distribution across the vortex axis at radial location $r = 1$.

where $\mathrm{Re}_c = cU/\nu_f$. Hence, Eq. (1) and Eq. (2) may be written in a dimensionless form as

$$\mathbf{u}_f = \frac{S}{r}\left(1 - e^{-\eta}\right)\bar{e}_\theta + \left(1 - \frac{C_D e^{-\eta}}{16\pi z}\right)\bar{e}_z. \tag{4}$$

$$p_f = 1 - \frac{\mathrm{Eu}_v}{r^2}\left[\left(1 - e^{-\eta}\right)^2 + 2\eta\left(\mathrm{Ei}\left(\eta\right) - \mathrm{Ei}\left(2\eta\right)\right)\right], \tag{5}$$

using three dimensionless parameters: the wing's drag coefficient

$$C_D = \frac{D}{\frac{1}{2}\rho_f U^2 c^2}, \tag{6}$$

the vortex swirl number

$$S = \frac{\Gamma}{2\pi c U}, \tag{7}$$

and the *vortex Euler number*

$$\mathrm{Eu}_v = \frac{\rho_f \Gamma^2}{8\pi^2 c^2 p_0} = \frac{\frac{1}{2}\rho_f U^2 S^2}{p_0}, \tag{8}$$

which signifies the ratio between the dynamic pressure drop and the total pressure.
Fig. 1 demonstrates the relation between Eu_v and the pressure field around the idealized trailing vortex; an increase of Eu_v manifests in lower absolute pressures at the origin of the vortex. The derived pressure field is used hereafter to couple the Lagrangian droplet transport with the thermodynamic gradients induced by the vortical flow. We also consider the vortex to be adiabatic; hence, one may couple the temperature field within the vortical viscous core to the pressure field

$$\tilde{T}_f = T_0\left(\frac{\tilde{p}_f}{p_0}\right)^{2/7}. \tag{9}$$

The temperature field outside the droplet is crucial for finding the droplet temperature, as it is dictated by, among other mechanisms, heat diffusion to the droplet.

2.2 Lagrangian equations

Maxey and Riley [18] formulated the generalized equations of motion for small particles in nonuniform, unsteady flows; they considered both gravity, drag, virtual mass, and the Basset "history" force. This study concerns the motion of a small liquid droplet in a gaseous medium; as such the particle-medium density ratio is large, and the droplet's characteristic length is much smaller relative to the vortex

viscous core size. Hence, we neglect the forces due to undisturbed flow, virtual mass, Faxen's drag correction, rotational inertia, and particle history terms. Additionally, we do not account for gravity and assume a linear drag term; the influence of both on the droplet dynamics will be relaxed and examined in future studies. We may now reduce the general form of the equations to the following:

$$\frac{d\mathbf{x_p}}{dt} = \mathbf{u_p}, \tag{10}$$

$$\frac{d\mathbf{u_p}}{dt} = \frac{\mathbf{u_f} - \mathbf{u_p}}{\mathrm{Stk}_0 d_p^2}, \tag{11}$$

where $\mathbf{x_p}$ and $\mathbf{u_p}$ are the droplet location and velocity vectors in the vortex frame of reference, respectively. d_p is the particle diameter normalized by its initial diameter d_0, and

$$\mathrm{Stk}_0 = \frac{\tau_{p,0}}{\tau_f} = \frac{U\rho_p d_0^2}{18\mu_f c} \tag{12}$$

is the *droplet initial Stokes number* – the ratio between the particle's initial relaxation time and free-stream flow time scale.

The size of the Lagrangian particle is governed by heat and mass transfer processes. Kulmala [19, 20] formulated the diffusive mass transfer at the droplet-gas interface for a quasi-stationary case while assuming that the medium is an ideal gas, the droplet-gas interface is saturated and a zeroth-order mass fraction profiles around the droplet. Although droplet ventilation may enhance the mass transfer out of the droplet, we aim to isolate the role of mass diffusivity and consider it as the primary transfer mechanism. In terms of droplet diameter, the mass equation is

$$\frac{d(d_p^2)}{dt} = \frac{4\rho^*_{v,\infty}}{9\mathrm{ScStk}_0\rho_f} \ln\left(\frac{p_0 p_f - p_{v,p}}{p_0 p_f - p_{v,\infty}}\right); \tag{13}$$

Sc is the non-dimensional Schmidt number, $\rho^*_{v,\infty}$ is the vapor ideal gas density in ambient conditions, $p_{v,p}$ is partial vapor pressure at the particle interface, and $p_{v,\infty}$ is the ambient partial vapor pressure. The difference between the vapor partial pressure at the interface and the vapor partial pressure at the far field dictates the mass flux to and from the droplet. Thus, we shall estimate both by assuming the Lagrangian particle consists of pure liquid water and the gaseous media is an air-vapor mixture with a relative humidity of ϕ. The diffusive driving force reduces to a single dimensionless number, the mass transfer coefficient C_m [12]; its generalized term is

$$\frac{p_0 p_f - p_{v,p}}{p_0 p_f - p_{v,\infty}} = 1 + \frac{\phi\, p_{sat}(T_0) - p_{sat}\left(\tilde{T}_p\right)}{p_0 p_f - \phi\, p_{sat}(T_0)} = 1 + C_m. \tag{14}$$

T_0 is the far-field carrier fluid temperature, $\tilde{T}_p$ is the (dimensional) droplet temperature, and $p_{sat}(T)$ is the vapor saturation pressure at a given temperature. The mass transfer coefficient sign and value indicate the nature of the mass transfer: evaporation occurs when $C_m < 0$ and the droplet interface vapor pressure is higher than far-field pressure, condensation occurs for $C_m > 0$ and the far-field vapor pressure is higher than the droplet interface pressure, whilst the mass flux is proportional to the transfer coefficient value $\dot{m} \propto |C_m|$.

The droplet temperature is regulated by heat conduction and convection to the carrier medium at the droplet surface, the sensible heat stored within it, and heat advection due to mass transport. One may derive [13] the normalized energy conservation equation for a single droplet assuming a zeroth-order temperature profile around the droplet. First, we introduce the non-dimensional temperature

$$\theta = \frac{\tilde{T} - T_0}{T_{sat}(p_0) - T_0} = \frac{\tilde{T} - T_0}{\Delta T_0}, \tag{15}$$

where $T_{sat}(p_0)$ is the vapor saturation temperature at the ambient pressure. Now, the Lagrangian energy equation yields

$$\frac{d\theta_p}{dt} = \frac{2}{3d_p^2}\left[\mathrm{Ste}_0^* \frac{d(d_p^2)}{dt} + \frac{4c_{p,f}}{9\mathrm{PrStk}_0 c_{p,p}}\left(\theta_f(\mathbf{x_p}) - \theta_p\right)\right], \tag{16}$$

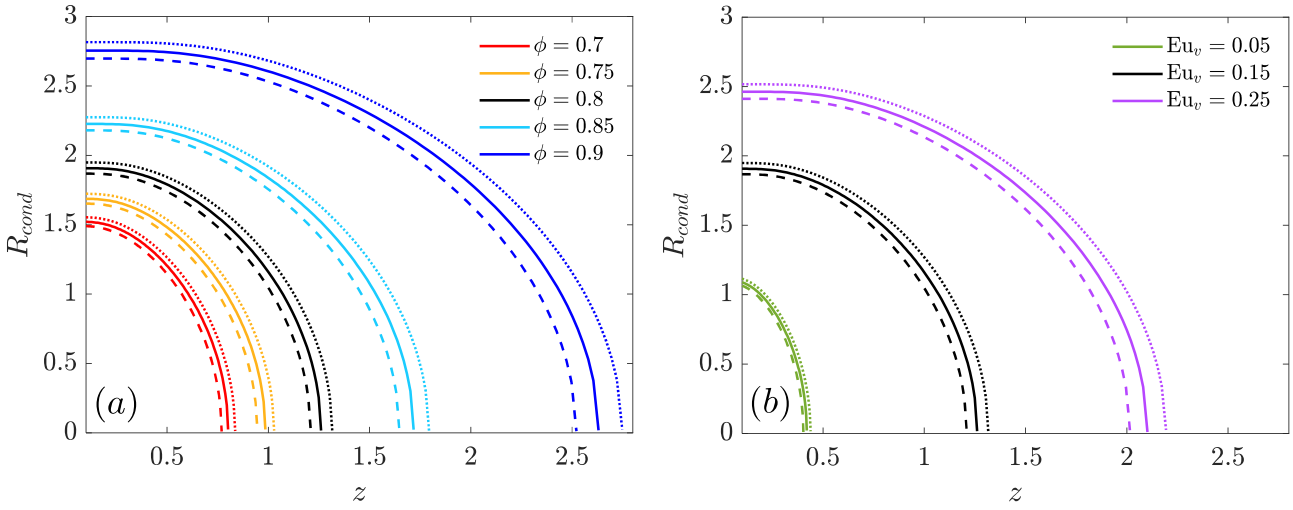

Figure 3 – Condensation core radius R_{cond} along the vortex axis for different vortex Euler numbers, relative humidities, and ambient temperatures. (a) Constant Euler number $\mathrm{Eu}_v = 0.15$ and varying relative humidities ϕ. (b) Constant air relative humidity $\phi = 0.8$ and varying vortex Euler numbers Eu_v. Dashed lines denote results obtained for ambient temperature of $T_0 = 290K$, while solid and dotted lines denote results obtained for $T_0 = 280K$ and $T_0 = 274K$, correspondingly.

where $\theta_f(\bar{x}_p)$ is the normalized carrier temperature at the droplet location, $c_{p,f}$ is the carrier fluid heat capacity, $c_{p,p}$ is the droplet heat capacity, $\mathrm{Pr} = c_{p,f}\nu_f/\rho_f k_f$ is the dimensionless Prandtl number. We also introduce a *modified Stefan number*, defined here as the ratio between the droplet substance's latent heat of evaporation and sensible heat maxima

$$Ste_0^* = \frac{L}{c_{p,p}\Delta T_0}, \tag{17}$$

denoting the latent heat of vaporization as L.
Both the thermodynamic conditions and the vortex properties may affect the mass transfer coefficient C_m field within it. The pressure drop due to the rotating flow may give rise to distinct condensation zones within the vortex core; the following section analyzes the influence of the dynamics of Lagrangian water droplets in and around vortices sustaining such conditions.

3. Results

3.1 Condensation core

The interaction between ambient thermodynamic conditions and localized variations induced by the vortex dictates the behavior of the mass transfer coefficient, potentially leading to a change in its sign near the vortex center. Namely, given the right conditions, condensation initiates in the vortex viscous core – as exhibited in many natural phenomena and industrial applications. Fig. 3 illuminates the relation between ambient properties and the evolving condensation core of the vortex. Near the wing, where z tends to 0, the condensation core reaches the maximal radial value. However, as the circulation decays along the vortex axis, a decrease in pressure drop occurs. Thus, the condensation core radius progressively shrinks, and eventually, far from the wing, the core disappears as expected. The influence of air relative humidity is depicted in Fig. 3 (a). Lower relative humidity leads to smaller condensation cores that decay rapidly along the vortex axis. Moreover, a nonlinear relation between the changes in the relative humidity and the core size emerges; the core size significantly increases and subsequently diverges as $\phi \to 1$. Fig. 3(b) illustrates how the vortex Euler number, representing the ratio between ambient and dynamic pressures within the vortex, affects the behavior of the condensation core. As expected, lower Euler values result in smaller cores. Notably, the values of the vortex Euler number are constrained by physical considerations. For instance, when $Eu > 0.25$, the pressure at the vortex center $p_f(r = 0)$ drops below absolute zero, an impossible thermodynamic state in gases. Realistically, the limit of physically possible trailing vortices is significantly lower. The

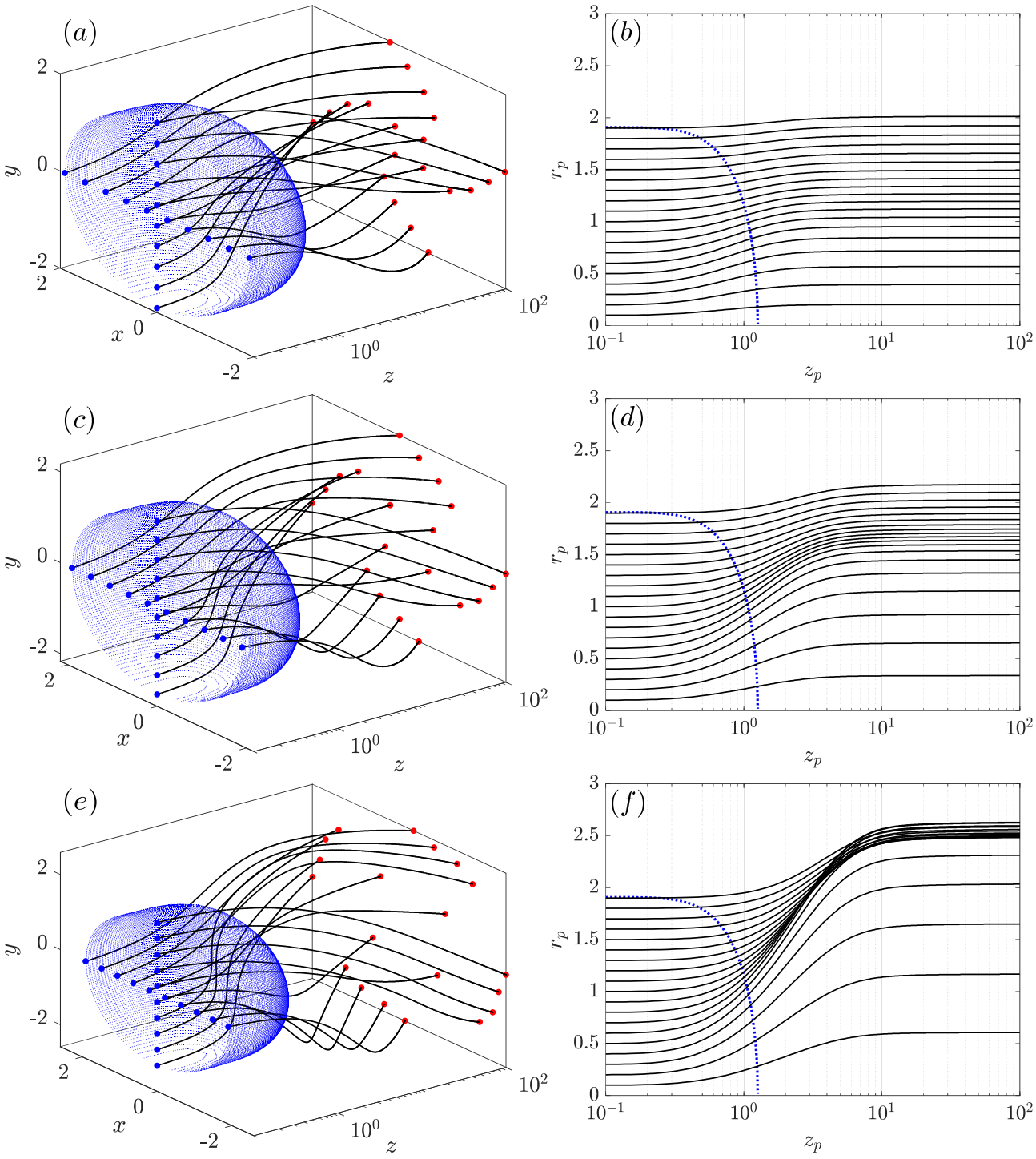

Figure 4 – Selected results of the Lagrangian model for droplets of various initial Stokes numbers: (a-b) $\mathrm{Stk}_0 = 0.1$, (c-d) $\mathrm{Stk}_0 = 1$, and (e-f) $\mathrm{Stk}_0 = 10$. The condensation core is illustrated by a blue ellipsoid, marking the edges of the region in which condensation occurs. LHS panels (a),(c), and (e) present the three-dimensional trajectories of droplets placed at equal distances along x and y axes inside the condensation core. RHS panels (b),(d), and (f) present the radial location of the droplets as a function of their location along the vortex axis.

effect of ambient temperatures in the range $T_0 = 274K - 290K$ is also explored and presented in Fig. 3. Smaller cores, corresponding to lower Eu_v or ϕ values, are less influenced by temperature changes. However, given larger cores, the ambient temperature impact becomes more pronounced, though still relatively minor compared to other parameters. However, the air relative humidity is strongly temperature-dependent, indirectly influencing the characteristics of the condensation core.

3.2 Droplet dynamics

The Lagrangian governing equations presented in sec. 2 suggest that one may characterize the complete dynamic and thermal behavior of a droplet in the vicinity of idealized trailing vortices in terms of four state variables $X_p = \left[\mathbf{x_p}, \mathbf{u_p}, \mathbf{d_p^2}, \theta_\mathbf{p}\right]$. The complex coupling between the external, vortex-induced forcing and the droplet's response gives rise to a nonlinear dynamic system,

$$\dot{X}_p = F(X_p, \dot{X}_p, ...) \ . \tag{18}$$

While aiming to investigate the system's dynamic response, the nonlinear ODE system will be solved numerically using an adaptive time-stepping RK4 scheme.

Since we seek to study the dynamics of water droplets within trailing vortices wherein condensation cores are forming, the air's thermodynamic properties are fixed at $p_0 = 1atm$, $T_0 = 280K$, and $\phi = 0.8$. Here we focus our discussion on the influence of the droplet's properties, i.e., initial location $\mathbf{x_{p,0}}$ and Stk_0, and thus set the vortex flow properties to be constant: $\mathrm{Eu}_v = 0.15$,$S = 1$,$C_D = 0.05$. Furthermore, the droplet area will be limited to $d_p^2 \geq 0.1$. Droplets crossing these thresholds are eliminated from the simulation; the mass equation, Eq. (13), cannot capture the droplet's complete drying without imposing an arbitrary threshold on the droplet's size.

Fig. 4 illustrates selected results of the Lagrangian model for droplets with various initial Stokes numbers: (a-b) $\mathrm{Stk}_0 = 0.1$, (c-d) $\mathrm{Stk}_0 = 1$, and (e-f) $\mathrm{Stk}_0 = 10$. In each case, 20 droplets are distributed along the x and y axes inside the condensation core at equal distances from each other, all placed at $z = 0.1$. An initial no-slip condition is assumed, as the droplet's initial velocity is set to be equal to the local flow velocity. Similarly, the droplets are considered to maintain thermal equilibrium with the surrounding air, $\theta_p(\mathbf{x_p}) = \theta_\mathbf{f}$. The initial Stokes number is determined by both the flow regime and droplet size; the latter is dictated by the nucleation mechanism and is coupled to the thermodynamic conditions at nucleation inception.

For initial Stokes numbers below unity ($\mathrm{Stk}_0 < 1$), Fig. 4(a-b) reveals that the droplets retain scattered distribution without notable clustering. Their spread radius slightly exceeds the initial condensation core radius, indicating a relatively even dispersion throughout the vortex flow. However, clustering phenomena become more apparent as the initial Stokes number reaches unity ($\mathrm{Stk}_0 = 1$). Fig. 4(d) highlight that this clustering primarily occurs when droplets exit the condensation core region, typically between $z = 1$ and $z = 5$. Beyond $z = 10$, the droplets' radial position stabilizes as they steadily swirl within the vortex, ultimately undergoing complete evaporation.

With further increases in the initial Stokes number, particularly surpassing $\mathrm{Stk}_0 > 1$, clustering becomes more pronounced. Such droplets tend to aggregate around specific radial locations, forming dense clusters with distinct spatial patterns. In the case of $\mathrm{Stk}_0 = 10$, Fig. 4(f) reveals that the clustering radius is expanding, surpassing the initial condensation core radius. The resulting pattern resembles an annular formation surrounding the core of the trailing vortex, with droplets accumulating around a specific radius. Such behavior holds significant implications for the transport and dispersion of droplets within vortical flows. This result implies that a proper analysis of the droplet dynamics must incorporate a model accounting for droplet-droplet interactions, e.g., collision, coalescence, and grouping.

4. Conclusions

A mathematical analysis of discrete droplet dynamics within a Batchelor vortex was conducted, revealing the complex coupling between the droplet motion and the thermodynamic gradients generated by the vortex. A Lagrangian approach is used to analyze the coupling between droplet motion and the flow field generated by the vortex. Under certain thermodynamic and hydrodynamic conditions, droplets may undergo evaporation and condensation when circulating the vortex core due to sharp changes in the environmental conditions induced by the vortex. We evaluated the pressure drop due to the vortical flow and quantified it using a non-dimensional vortex Euler number Eu_v. The resultant gradients may be large enough to initiate condensation within the vortex core. The onset of condensation was studied by defining a mass transfer coefficient C_m, indicating the direction and extent of mass transfer to the Lagrangian water droplet. Our study uncovered a distinct clustering phenomenon linked to the initial Stokes number, with droplets showing a tendency to aggregate at

higher Stokes numbers. In summary, the presented model offers valuable insights into droplet dynamics within trailing vortices, contributing to improved modeling and prediction of droplet transport phenomena across various fields, from atmospheric science to engineering applications.

Acknowledgments

This research was supported by the ISRAEL SCIENCE FOUNDATION (grant No. 1762/20).

Contact Author Email Address

Corresponding author (Yuval Dagan) email: yuvalda@technion.ac.il.

Copyright Statement

References

[1] D. I. Pullin and P. G. Saffman. Vortex dynamics in turbulence. *Annu. Rev. Fluid Mech.*, 30:31–51, 1 1998.

[2] J. Dávila and J. C.R. Hunt. Settling of small particles near vortices and in turbulence. *J. Fluid Mech.*, 440:117–145, 8 2001.

[3] N. W. Chakroun, S. J. Shanbhogue, Y. Dagan, and A. F. Ghoniem. Flamelet structure in turbulent premixed swirling oxy-combustion of methane. *Proc. Combust. Inst.*, 37(4):4579–4586, 2019.

[4] Y. Dagan, D. Katoshevski, and J. B. Greenberg. Similarity solutions for the evolution of unsteady spray diffusion flames in vortex flows. *Combust. Sci. Technol.*, 190(6):1110–1125, 2018.

[5] Y. Dagan, E. Arad, and Y. Tambour. The evolution of local instability regions in turbulent non-premixed flames. *J. Fluid Mech.*, 803:18–50, 2016.

[6] S. Taamallah, Y. Dagan, N. Chakroun, S. J. Shanbhogue, K. Vogiatzaki, and A. F. Ghoniem. Helical vortex core dynamics and flame interaction in turbulent premixed swirl combustion: A combined experimental and large eddy simulation investigation. *Phys. Fluids*, 31(2):25108, 2019.

[7] Y. Dagan, N. W. Chakroun, S. J. Shanbhogue, and A. F. Ghoniem. Role of intermediate temperature kinetics and radical transport in the prediction of leading edge structure of turbulent lean premixed flames. *Combust. Flame*, 207:368–378, 2019.

[8] Y. Dagan, E. Arad, and Y. Tambour. On the dynamics of spray flames in turbulent flows. *Proc. Combust. Inst.*, 35(2):1657–1665, 2015.

[9] Y. Dagan. Settling of particles in the vicinity of vortex flows. *At. Sprays*, 31:33–45, 2021.

[10] O. Avni and Y. Dagan. Dynamics of evaporating respiratory droplets in the vicinity of vortex dipoles. *Int. J. Multiph. Flow*, 148:103901, 3 2022.

[11] O. Avni and Y. Dagan. Dispersion of free-falling saliva droplets by two-dimensional vortical flows. *Theor. Comput. Fluid Dyn.*, 36:993–1011, 12 2022.

[12] O. Avni and Y. Dagan. Droplet dynamics in burgers vortices. i. mass transport. *Phy. Rev. Fluids*, 8:083604, 8 2023.

[13] O. Avni and Y. Dagan. Droplet dynamics in burgers vortices. ii. heat transfer. *Phys. Rev. Fluids*, 8:083605, 8 2023.

[14] R. Jugier, J. Fontane, L. Joly, and P. Brancher. Linear two-dimensional stability of a lamb-oseen dipole as an aircraft wake model. *Phy. Rev. Fluids*, 5(1):014701, 2020.

[15] M. Atias and D. Weihs. On the motion of spray drops in the wake of an agricultural aircraft. *At. Sprays*, 1:21–36, 1985.

[16] G. K. Batchelor. Axial flow in trailing line vortices. *J. Fluid Mech.*, 20:645–658, 12 1964.

[17] P. G. Saffman. *Vortex Dynamics*. Cambridge University Press, 1 1993.

[18] M. R. Maxey and J. J. Riley. Equation of motion for a small rigid sphere in a nonuniform flow. *Phys. Fluids*, 26(4):883–889, 1983.

[19] M. Kulmala, A. Majerowicz, and P. E. Wagner. Condensational growth at large vapour concentration: Limits of applicability of the mason equation. *J. Aerosol Sci.*, 20:1023–1026, 1989.

[20] M. Kulmala and T. Vesala. Condensation in the continuum regime. *J. Aerosol Sci.*, 22:337–346, 1 1991.